IEEE Photonics Journal
An IEEE Photonics Society Publication

Open Access

Broadband Visible Light Emission From Nominally Undoped and Cr^{3+} Doped Garnet Nanopowders

Volume 6, Number 4, August 2014

G. Bilir
G. Ozen
M. Bettinelli
F. Piccinelli
M. Cesaria
B. Di Bartolo

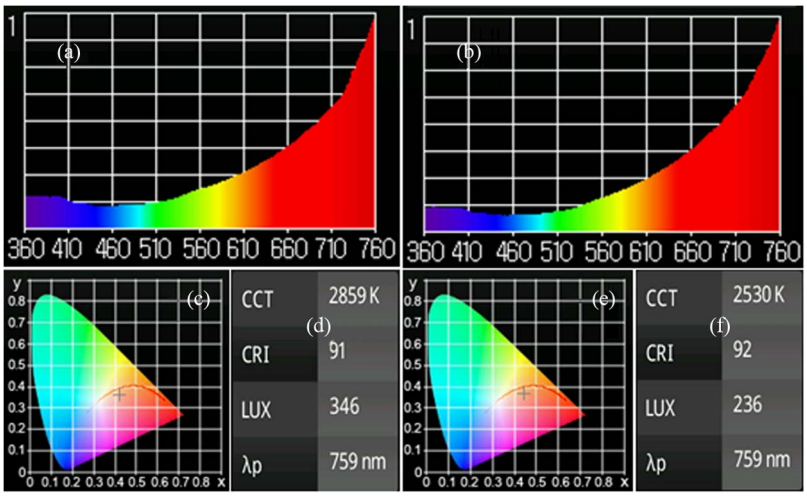

DOI: 10.1109/JPHOT.2014.2337873
1943-0655 © 2014 IEEE

Broadband Visible Light Emission From Nominally Undoped and Cr^{3+} Doped Garnet Nanopowders

G. Bilir,[1,2] G. Ozen,[1] M. Bettinelli,[3] F. Piccinelli,[3] M. Cesaria,[4] and B. Di Bartolo[2]

[1]Department of Physics, Istanbul Technical University, 34469 Istanbul, Turkey
[2]Department of Physics, Boston College, Chestnut Hill, MA 02467-3804, USA
[3]Luminescent Materials Laboratory, University of Verona, 37134 Verona, Italy
[4]Department of Physics, Università del Salento, 73100 Lecce, Italy

DOI: 10.1109/JPHOT.2014.2337873

Manuscript received May 10, 2014; revised June 28, 2014; accepted July 1, 2014. Date of publication July 22, 2014; date of current version July 28, 2014. Corresponding author: G. Bilir (e-mail: bilir@bc.edu).

Abstract: Synthetic garnet nanopowders of $Y_3Al_5O_{12}$ (YAG) and $Gd_3Ga_5O_{12}$ (GGG) were produced, and the occurrence of a broadband bright visible emission by nominally undoped YAG and GGG and Cr^{3+} doped GGG, depending on the environment pressure, as well as exciting on the pumping power, was demonstrated. The results indicate that high-intensity infrared laser irradiation in samples not only leads to heating (melting effects) but also produces visible broadband emission. Low pressure of the powders' environment favors the white light emission by lowering the threshold pumping power. A hypothesis on the nature of the emission is presented.

Index Terms: Garnets, nanocrystals, white light emission, laser diode excitation.

1. Introduction

White Light (WL) optical emission from inorganic materials is an important research subject of research emerged in the last decade may find numerous applications, in the fields of lighting and signaling. The majority of the papers that have appeared in the literature have dealt with WL obtained by using a blue or an ultraviolet (UV) light emitting diode exciting one or more suitable and efficient phosphors (only a yellow phosphor, both yellow and red phosphors or both green and red phosphors), with the combination of the emitted radiations originating the WL [1]. According to this strategy i) yellow phosphors enable to get WL with high efficiency but with low color rendering index (CRI), ii) yellow and proper red phosphors let achieve WL with appropriate CRI and moderate luminescence efficiency and iii) emission by green and red phosphors provides WL with high CRI but with low efficiency [2].

Other approaches exploit an up-conversion mechanism with a suitable near-infrared (NIR) source excitation with high power above a certain threshold and nano-crystalline powders of a transparent host material doped with lanthanide ions [3]. In several cases, very bright white or yellowish light was observed, corresponding to an intense and broadband emission-band covering almost the whole visible region [4]–[9]. The broadband emission was assigned to blackbody thermal emission in some cases, to charge transfer luminescence in other cases, or to a combination of these two processes. As for the materials used, previously reported WL production

TABLE 1

Garnet samples under investigation

Sample	Synthesis	Doping	Metal source and purity	Metal source and purity	Dopant source and purity
$(YAG)_{Pech}$	Pechini	Nominally undoped	$Y(NO_3)_3{\cdot}6H_2O$ (99.8%)	$Al(NO_3)_3{\cdot}9H_2O$ (99.999%)	
$(YAG)_{co}$	Coprecipitation	Nominally undoped	$Y(NO_3)_3{\cdot}6H_2O$ (99.8%)	$NH_4Al(SO_4)_2{\cdot}12H_2O$ (>99%)	
GGG-U	Pechini	Nominally undoped	Gd_2O_3 (99.99+%)	$Ga(NO_3)_3{\cdot}8.31H_2O$ (99.999%)	
GGG:Cr	Pechini	1 mol% Cr^{3+} (substituting Ga^{3+})	Gd_2O_3 (99.99+%)	$Ga(NO_3)_3{\cdot}8.31H_2O$ (99.999%)	$Cr(NO_3)_3{\cdot}9H_2O$ (99.99+%)

stemmed from transparent host materials co-doped with rare earth (RE) ions or including RE ions as stoichiometric components.

The garnets $Y_3Al_5O_{12}$ (YAG) and $Gd_3Ga_5O_{12}$ (GGG) are well known in nano-crystalline form [10] and are among the most widely used laser host materials [11] because of their hardness, general stability against chemical and mechanical changes, optical isotropy, good thermal conductivity and low-thermal expansion, high-optical transparency, low-acoustic loss, high threshold for optical damage and high receptiveness to rare earth ions. While YAG has slightly better thermal and optical properties than GGG, GGG is more easily available and in better crystalline quality than YAG.

To the best of our knowledge, no study is available examining the possibility to generate broad-band WL emission by nominally un-doped or transition-metal-doped insulating oxide materials. Hence, this paper demonstrates the occurrence of broadband bright visible emission, depending on environment pressure and pumping power, by either nominally un-doped YAG and GGG or Cr^{3+} doped GGG nano-crystalline samples excited by monochromatic CW infrared light (803.5 nm).

2. Experimental Details

2.1. Synthesis Procedure

To produce powders with grain size in the range of nanometers, the Pechini method [12] and the co-precipitation approach [14] were exploited. The former method besides being simple and inexpensive, has the advantage of providing reproducible and monodispersed samples. It is a common method for the synthesis of metal oxide materials with the aid of an organic polymer and a chelating agent to form a polyesteric network which can be eliminated by thermal treatment.

Four nano-crystalline garnet samples were investigated in the present study:

i) two samples of nominally undoped YAG, briefly named $(YAG)_{Pech}$ and $(YAG)_{co}$, the Pechini method [15], and by co-precipitation [13], respectively;
ii) one nominally undoped GGG sample, named $(GGG)_{Pech}$ hereafter, prepared by the Pechini method [16];
iii) one Cr-doped GGG sample, named GGG:Cr hereafter, with 1 mol% Cr^{3+}(substituting Ga^{3+}).

The reagents used in the synthesis are given in Table 1. The heat treatment was carried out for 16 hours at 800 °C for the samples prepared by the Pechini method, and 3 hours at 900 °C for the YAG sample made by coprecipitation. The metallic precursors were obtained from Sigma–Aldrich, apart from $Al(NO_3)_3 \cdot 9H_2O$ (Alfa Aesar).

2.2. Structural Characterization

The powder samples were ground in a mortar and then deposited in a low-background sample stage for the X-ray powder diffraction (XRD) pattern collection. XRD patterns were measured with a Thermo ARL X'TRA powder diffractometer, operating in Bragg–Brentano geometry

(to increase intensity and angular resolution), equipped with a Cu-anode X-ray source ($K\alpha$, $\lambda = 1.5418$ A) and using a Peltier Si(Li) cooled solid state detector. The patterns were collected with a scan rate of 0.003°/s, time of exposure 9.0 s/step and 2θ range of 24–90°. The phase identification was performed with the PDF-4 + 2008 database provided by the International Centre for Diffraction Data (ICDD).

The crystallite size of the single phase samples were evaluated using the Williamson–Hall method.

2.3. Spectroscopic Measurements

The continuous emission spectra of the samples were obtained by pumping the samples with the output of a Laser Drive Inc. Model LDI-820 diode laser operated at 803.5 nm. The signal emitted by the samples was directed toward the entrance slit of a 1 m McPherson Model 2051 monochromator and chopped at a frequency of 250 Hz before entering the slit. The monochromator provided a resolution 0.8 Å with the slits set at 50 μm and a wavelength reproducibility of 0.1 Å.

The optical signal was detected by a Hamamatsu R1387 photomultiplier tube with an S20 response, sent to a EG&G Model 5210 lock-in amplifier and recorded in a computer.

The temporal evolution (decay and rise patterns) of the visible broadband emission intensity of all the samples was measured by employing a shutter to switch on or interrupt the diode laser beam and a Tektronix Model TDS3052B oscilloscope.

The samples were mounted on the cold finger of a closed cycle Helium refrigerator. This system uses a Janis Research Model RD Dewar connected with a Leybold Model RW2 compressor. The temperature of the cold finger was controlled by using a Lake Shore Cryotronics 805 Model controller and could be changed from 30 to 300 K.

An Avantes AvaLight-Hal-Cal calibration light source was used to correct our spectra for the sensitivity of our system.

An Allied Scientific Pro ASP-MK350 Model Illuminance Meter was used to measure the CIE (International Commission on Illumination) coordinates, the CCT (Correlated Color Temperature), the CRI (Color Rendering Index), the luminous flux, and to view the spectrum of the WL.

3. Results and Discussions

3.1. Structural Characterization of the Samples

The X-ray patterns corresponding to the four samples are shown in Fig. 1. The results of the structural investigation are summarized in Table 2.

i) The $(YAG)_{co}$, $(GGG)_{Pech}$ and GGG:Cr samples were found to be nano-crystalline, single phase with a cubic garnet structure and with crystallite sizes in the range 50–80 nm (Table 2);

ii) The $(YAG)_{Pech}$ sample was found to contain about 7 mass % of a slightly distorted garnet phase with a stoichiometry close to $Y_{3.03}Al_{4.97}O_{12}$ [17] and, even if the average size of such mixed phase sample was not determined, peak broadening indicates its nano-crystalline nature. $Y_{3.03}Al_{4.97}O_{12}$ arises from $Y_3Al_5O_{12}$ by substitution of a small portion of Al^{3+} ions, occupying the trigonally distorted octahedral site (with S_6 symmetry), with Y^{3+} ones. Due to the mismatch of the ionic radii of Al^{3+} and Y^{3+}(the latter is larger than the former), the cell edge of $Y_{3.03}Al_{4.97}O_{12}$ is bigger than the one of $Y_3Al_5O_{12}$. As a consequence, the diffraction peaks of $Y_{3.03}Al_{4.97}O_{12}$ are shifted towards lower 2 theta values, with respect to the ones of $Y_3Al_5O_{12}$. (see Fig. 1(a)).

It has been reported in the literature that nano-crystalline garnet materials show weak aggregation of the particles and the relatively small particle size is accompanied by significant porosity and surface area [18].

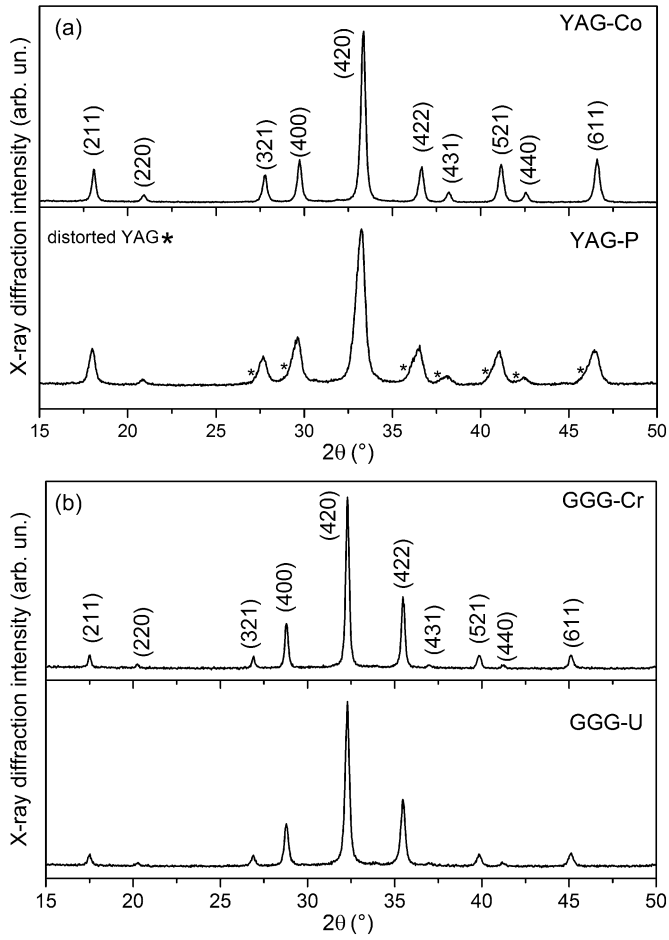

Fig. 1. XRD patterns of (a) YAG and (b) GGG samples.

TABLE 2

Structural characterization of the garnet samples under investigation

Sample	Phase purity	Particle size
$(YAG)_{Pech}$	Not single phase: presence of 7 weight % of distorted YAG	n.a.
$(YAG)_{co}$	Single phase	55 nm
GGG-U	Single phase	53 nm
GGG:Cr	Single phase	78 nm

3.2. Spectroscopic Investigation of the Samples

The onset of a broad emission band extending from 400 to 900 nm was observed peaking in the anti-Stokes side of the exciting laser line (see Fig. 2) with the samples under a pressure of 0.032 mbar, the cold finger at 300 K and the laser exciting power raised above a certain threshold (0.2 W for GGG:Cr and 1.05 W for $(YAG)_{co}$).

In the experimental conditions described above, a broad band emission could be visually observed with the maximum exciting power of 3.25 W for the other two samples $(YAG)_{Pech}$ and $(GGG)_{Pech}$, but its persistence was very short and no meaningful measurements could be carried out. For these reasons, in what follows, only the emission properties of the samples GGG:Cr and

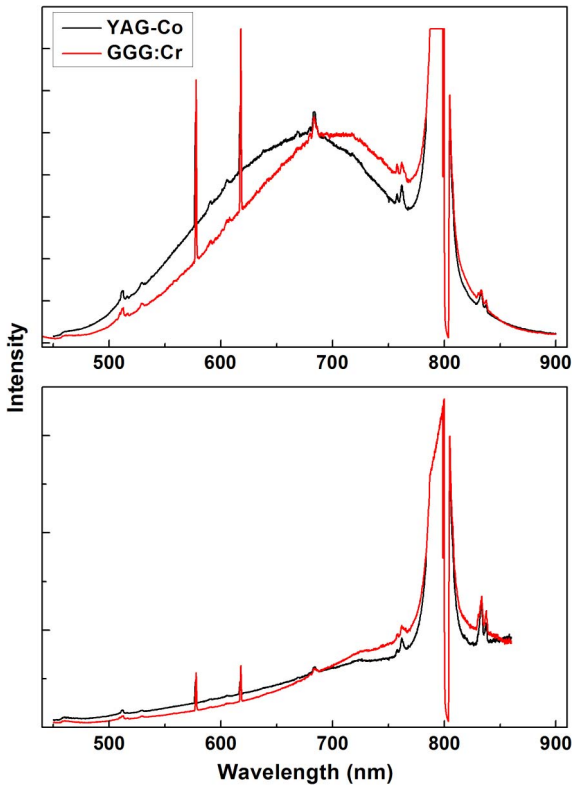

Fig. 2. (a) Spectral profiles of the broad band emission for $(YAG)_{co}$ and GGG:Cr. (b) Corrected spectra of YAG-Co and GGG-Cr for system response.

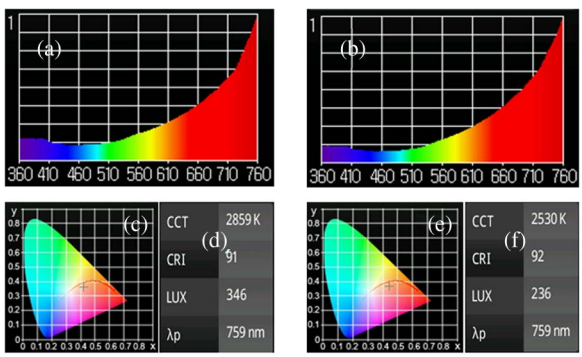

Fig. 3. (a) Measured spectrum for $(YAG)_{co}$ by using illuminance meter. (b) Measured spectrum for GGG:Cr by using illuminance meter. (c) CIE coordinates for $(YAG)_{co}$. (d) CIE coordinates for GGG:Cr. (e) CCT, CRI, and illuminance values for $(YAG)_{co}$. (f) CCT, CRI, and illuminance values for GGG:Cr.

$(YAG)_{co}$ will be dealt with. Accordingly, Fig. 2(a) reports the WL found emitted these two samples. The peak intensities are located at 680 and 700 nm for $(YAG)_{co}$ and GGG, respectively.

The spikes that appear in Fig. 2(a), superimposed to the WL band are due to the spurious modes of the laser.

The WL was incoherent and with no preferential spatial direction. Fig. 2(b) reports the spectra in Fig. 2(a) corrected for the system response and Fig. 3 presents the spectra of the WL emitted by the two samples measured by using an illuminance meter. We may note the similarity of the spectra in Figs. 2(a) and 3.

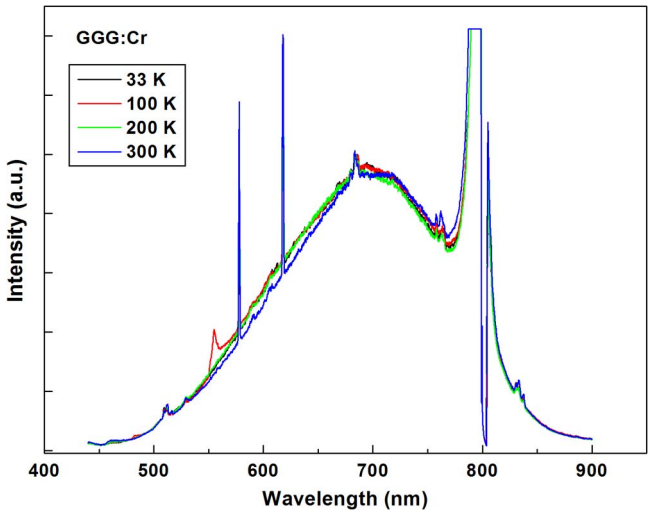

Fig. 4. Temperature evolution of the broad band emission of GGG:Cr in the range 33–300 K.

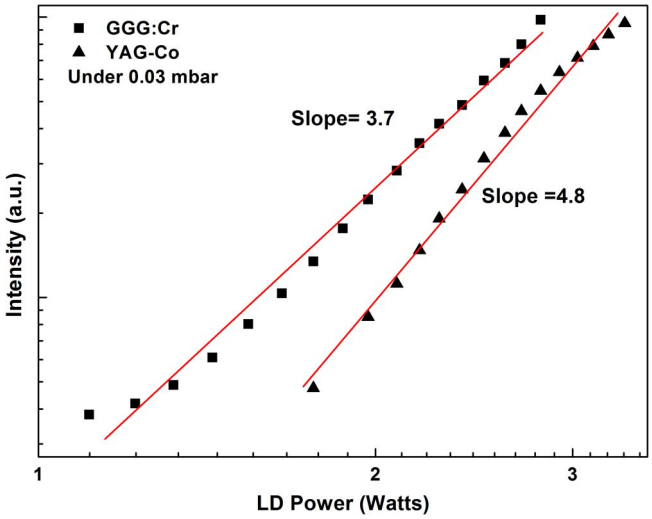

Fig. 5. Evolution of the broad band peak intensity as a function of the diode laser power for $(YAG)_{co}$ and GGG:Cr. The atmospheric pressure was 0.03 mbar.

The chromaticity coordinates were found to be $x = 0.42$ and $y = 0.36$ for $(YAG)_{co}$ and $x = 0.45$ and $y = 0.37$ for GGG:Cr. These values lie in the greenish yellow region and correspond to correlated color temperature (CCT) values of approximately 2859 and 2530 K with the CRI of 91 and 92, respectively (see Fig. 3).

We also measured the WL emitted by two samples when varying the temperature of the cold finger and noted that neither the profile nor the emission intensity appear to change significantly. This result, per se, indicates that the emitting part of the sample is at such high temperature that a change of temperature (see Fig. 4) of the cold finger has no relevant effect on the WL emission.

The emission intensity exhibits a dependence on the excitation power. The peak emission intensity increases with the laser power in a highly non-linear way, and the increase is more steep for $(YAG)_{co}$ than for GGG:Cr (see Fig. 5). In fact, the power dependence of the intensity can be approximated by $I = AP^n$, where I is the peak intensity, A is a constant, P is the diode laser power and the exponent n is 4.8 for $(YAG)_{co}$ and 3.7 for GGG:Cr.

These findings have relevance on the mechanism by which the 803.5 nm radiation is absorbed and deposited in the sample. Accounting for the intrinsic energy band gaps of the considered host materials (6.6 eV for YAG and 5.4 eV for GGG), no direct interband linear absorption could occur by the host material at the considered exciting photon energy (1.28 eV). However, the high intensity radiation provided by the laser diode may be expected to produce a multiphoton absorption.

Non resonant (i.e., without the presence of intermediate gap states) multiphoton absorption would require 5.07 and 4.21 incident photons for YAG and GGG, respectively. Based on the estimation of the exponent n occurring in the law $I = AP^n$ (see Fig. 5), a resonant multi-photon absorption is likely to occur for YAG [19]–[22].

As for the absorption mechanism in GGG:Cr, we need to consider the possible role played by the Cr^{3+} ion. The WL emission of the GGG:Cr sample has a weak tail in spectral region near the exciting wavelength that happens to fall in an absorption band of Cr^{3+} [23].

Investigations of GGG doped with Cr^{3+} ions report that such material strongly absorbs radiation with wavelength lower than 700 nm: two broad and intense absorption bands at 610 and 430 nm are typical for Cr^{3+} octahedrally-coordinated by O atoms [23]. Broadband emission by Cr^{3+} ion is known as due to the coupling between the electronic levels of the 3*d*-like electrons and the lattice vibrations and Cr^{3+} fluorescence properties are sensitive to the crystal field strength [24], [25]. The $^4A_2$ ground level and the excited levels ^2E and ^4T are involved in the emission dynamics. At low temperature the Cr^{3+} ion luminescence is dominated by the $^2E \rightarrow {}^4A_2$ transitions (with peaks at 730, 726, and 706 nm) [26], [27] and at room temperature a wide band occurs peaking at 719 nm.

Since our samples GGG:Cr and $(YAG)_{co}$ yield broadband visible emission with analogous features (see Fig. 2) and no temperature-dependence is exhibited by the broadband emission of the sample GGG:Cr (see Fig. 3), then the occurrence of the visible broadband emission cannot be ascribed to the Cr presence. That is, the similarities of the emission properties of $(YAG)_{co}$ and GGG:Cr suggest that the nature of the general emission mechanism may be the same in both materials.

The experimental findings indicate that the only nominally un-doped sample that shows stable broadband emission is $(YAG)_{co}$, fabricated by using relatively low purity starting source reagents of both Y and Al [$Y(NO_3)_3 \cdot 6H_2O$ (99.8%) and $NH_4Al(SO_4)_2 \cdot 12H_2O$ ($>$ 99%)]. On the other hand, no stable broad band emission was observed at atmospheric pressure by the samples $(GGG)_{Pech}$, fabricated by very high purity reagents [Gd_2O_3 (99.99+%) and $Ga(NO_3)_3 \cdot xH_2O$ ($x = 8.31$; 99.999%)], and $(YAG)_{Pech}$, produced by using a high purity reagent [$Al(NO_3)_3 9H_2O$ (99.999%)] and a low purity reagent [$Y(NO_3)_3 \cdot 6H_2O$ (99.8%)]. Even if the very different behavior of our samples deserves further investigation, the following remarks can be made based on our experimental study.

The GGG-based samples (GGG:Cr and $(GGG)_{Pech}$), were synthesized by the better approach but consist of nano-crystallites with different sizes (78 nm for GGG:Cr and 53 nm for $(GGG)_{Pech}$). This issue can be related to the Cr-dopant. In fact, while synthesis thermal-treatments induce thermally activated nucleation due to improved superficial mobility, Cr-doping can be active in promoting heterogeneous nucleation by enhanced density of nucleation sites. In fact, the smaller ionic radius of Cr^{3+} ions as compared to Gd^{3+} cations introduces lattice-potential well favoring dopant effectiveness as nucleation centre. Since larger nano-crystals exhibit improved crystalline quality, this refined structural order yield less defects which means reduction of the channels of non-radiative loss and, therefore, could result in measurable and stable broadband emission.

Turning to the YAG-based samples ($(YAG)_{co}$ and $(YAG)_{Pech}$), they were synthesized by different approaches and exhibited very different structural features: $(YAG)_{co}$ was single-phase with 55 nm-large nano-crystals and $(YAG)_{Pech}$ was not-single phase with distorted lattice. While Y-based precursors with equal purity were used to synthesize both samples, the used Al

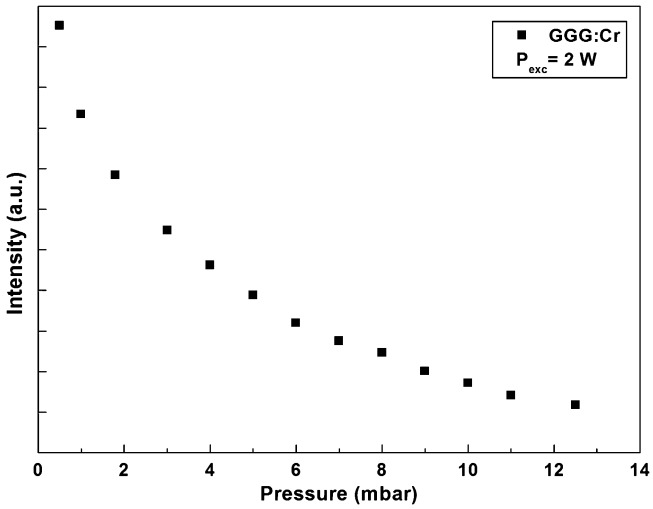

Fig. 6. Evolution of the broad band peak intensity as a function of the atmospheric pressure for GGG:Cr. The excitation power was 2 W.

precursors had very different purity (99.999% for $(YAG)_{Pech}$ and 99% for $(YAG)_{co}$). Even if the nature of these impurities is presently unknown, we point out that Cr^{3+}, Cu^{2+}, Fe^{3+} and other transition metal ions are common metallic impurities in nominally pure compounds containing Al^{3+} [28], [29]. Therefore, the overall minor purity of reagents may be responsible of the distorted phase of the sample $(YAG)_{Pech}$. Once again, the different density of structural defects could account for the lack of stable visible broadband emission by $(YAG)_{Pech}$, as compared to $(YAG)_{co}$.

Another contribution to the reduction/suppression of the visible broadband emission might be the water (H_2O) residing on the nano-particle surface, due to either synthesis residuals or adsorption in atmospheric pressure [30]. Since H_2O has a relatively broad absorption band peaking at 760 nm and at 800 nm its absorption coefficient is 0.02 cm^{-1} [31], it could contribute to the absorption of the 803.5 radiation. Under equal conditions of background pressure, the different surface-to-volume ratio of the GGG-based samples involves greater density of adsorbed water on the surface of the sample $(GGG)_{Pech}$ as compared to GGG:Cr, thus contributing to suppress broadband emission by $(GGG)_{Pech}$. Such conclusion is supported by the experimental finding that $(GGG)_{Pech}$ yields only unstable visible broadband emission at very high pumping power (nearly 3.25 W) under atmospheric pressure conditions. For what concerns $(YAG)_{Pech}$ and $(YAG)_{co}$ different water adsorption can only stem from the surface-characteristics, as induced by the synthesis procedure.

As for the dependence of the WL emission on the pressure present in the sample chamber Fig. 6 reports such pressure dependence for the GGG:Cr sample at the pumping power of 2 W; the WL intensity decreases sharply with increasing pressure. For the sample $(YAG)_{co}$, no experiment as a function of pressure was carried out, as the broadband emission is measurable only for the lowest available atmospheric pressures (below 0.1 mbar).

The pressure dependence of the broadband emission can be due to the adsorption of polar species on the sample surface and the scattering events involving the nano-powder surface and molecules of the background atmosphere that cause electron de-excitation and/or heating dissipation. The heating effects on the samples after their exposure to the laser beam are demonstrated by their partial melting that can be ascribed to the low thermal conductivity of nanomaterials and reduced melting temperature as compared to the bulk counterpart. In this regard an alternative or concurrent pressure-dependent de-excitation mechanism can be invoked based on the thermal conductivity of the nano-powders. This parameter is enhanced by the ambient pressure and reduced when this pressure is lowered. At low pressures, the crystallites are

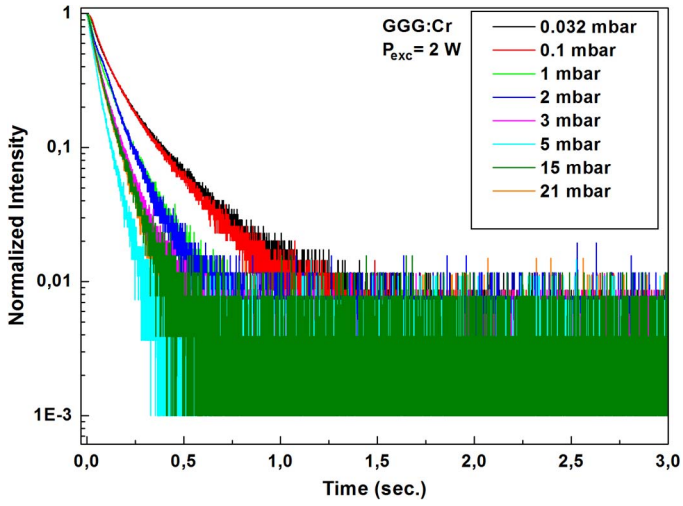

Fig. 7. Decay of the broadband emission intensity at 675 nm as a function of the atmospheric pressure for GGG:Cr at room temperature. The excitation power was 2 W.

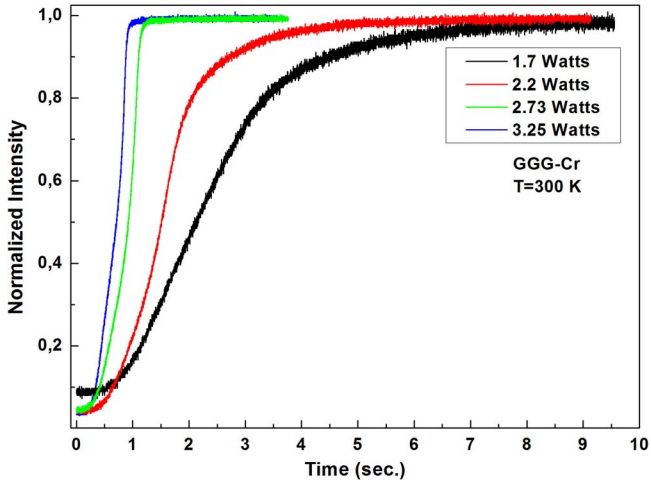

Fig. 8. Temporal rise of the broadband intensity at 675 nm as a function of the excitation power at ambient pressure (0.03 mbar).

more isolated from each other and from the cold finger and can reach higher temperatures favoring the emission of WL.

The decay patterns of the visible broadband emission of the sample GGG:Cr, measured under various pressure conditions, are shown in Fig. 7. Following the instantaneous interruption of the diode laser irradiation by a shutter, the emission intensity decays in a non-exponential way, with an e-folding time on the order of 0.1 s (see Fig. 7). However, the decay rate appears to be strongly affected by the pressure in the sample chamber, as the first e-folding time for GGG:Cr approximately changes from 50 to 150 ms for pressures varying from 21 to 0.032 mbar.

After the instantaneous opening of the shutter blocking the 803.5 nm CW excitation, the broadband intensity increases slowly as a function of the excitation pumping power (see Fig. 8). In all the cases the rise of the emission intensity is not fast, but takes up to a few seconds to reach a common steady-state value. The rise becomes faster when the power is increased. Similar results were obtained for the $(YAG)_{co}$ samples.

The active role of the de-excitation mechanisms aided by the background pressure is consistent with decay rate strongly affected by the atmospheric pressure and fast decreasing for

increasing pressure (see Fig. 6). Notably, while at the lowest background pressures the decay pattern is non-exponential, for increasing pressure nearly linear trend is approached. Since the decay accounts for both radiative and non-radiative processes and the contribution stemming from the background pressure is just an extrinsic non-radiative loss channel, such a finding suggests that just above the threshold pressure the decay time of the broadband emission is dominated by the material intrinsic mechanisms. High pumping power favors the onset of step-like build up of the broadband emission (see Fig. 7). Such an evidence suggests that this emission is related to state-filling and threshold-filling mechanisms. As increasing pumping power means an increasing population of the excited level; the emission intensity is expected to build up proportionally to the filling of the excited states. In this picture, at low pumping power, the insufficient level filling should account for the tailing-effect observed in the rise-time curves (see Fig. 7) corresponding to the lowest pumping-powers (1.7 and 2.2 W). The step-like increase of the WL onset for pumping power up 2.73 W can be indicative of a threshold filling-process.

4. Conclusion

Visible broadband emission is reported in the literature by materials at least doubly doped with different rare earth ions or including them as stoichiometric components. The present study demonstrates that this emission can be obtained by nominally undoped oxide materials and, for the first time, by transition-metal-doped insulating oxide materials. This study has presented the occurrence of broadband bright visible emission by either nominally un-doped YAG and GGG or Cr^{3+} doped GGG nano-crystalline samples excited by monochromatic CW infrared light (803.5 nm). It has also demonstrated the influence of the experimental conditions (synthesis approach, purity of the precursor powder, environment pressure and pumping power) in favoring or suppressing the broadband emission. Based on the analysis of the data and on our preliminary results [32], [33], it can be inferred that the observed broadband emission is due to a host dependent general mechanism.

Acknowledgement

The authors gratefully thank E. Viviani (Univ. Verona) for expert technical assistance.

References

[1] S. T. Tan, X. W. Sun, H. V. Demir, and S. P. Denbaars, "Advances in the LED materials and architectures for energy-saving solid-state lighting toward 'lighting revolution'," *IEEE Photon. J.*, vol. 4, no. 2, pp. 613–619, Apr. 2012.
[2] L. Chen, C. C. Lin, C. W. Yeh, and R. S. Liu, "Light converting inorganic phosphors for white-light emitting diodes," *Materials*, vol. 3, no. 3, pp. 2172–2195, 2010.
[3] V. Mahalingam *et al.*, "Bright white upconversion emission from $Tm^{3+}/Yb^{3+}/Er^{3+}$-Doped $Lu_3Ga_5O_{12}$ nanocrystals," *J. Phys. Chem. C*, vol. 112, no. 46, pp. 17745–17749, 2008.
[4] S. Redmond, S. C. Rand, X. L. Ruan, and M. Kaviany, "Multiple scattering and nonlinear thermal emission of Yb^{3+}, Er^{3+} : Y_2O_3 nanopowders," *J. Appl. Phys.*, vol. 95, no. 8, pp. 4069–4077, 2004.
[5] J. Wang, J. H. Hao, and P. A. Tanner, "Luminous and tunable white-light upconversion for YAG (Yb3Al5O12) and (Yb, Y)2O3 nanopowders," *Opt. Lett.*, vol. 35, no. 23, pp. 3922–3924, Dec. 2010.
[6] J. Wang and P. A. Tanner, "Upconversion for white light generation by a single compound," *J. Amer. Chem. Soc.*, vol. 132, no. 3, pp. 947–949, 2009.
[7] W. Stręk *et al.*, "White emission of lithium ytterbium tetraphosphate nanocrystals," *Opt. Exp.*, vol. 19, no. 15, pp. 14083–14092, Jul. 2011.
[8] W. Strek, Ł. Marciniak, D. Hreniak, and A. Łukowiak, "Anti-stokes bright yellowish emission of NdAlO3 nanocrystals," *J. Appl. Phys.*, vol. 111, no. 2, pp. 024305, Jan. 2012.
[9] R. K. Verma and S. B. Rai, "Continuum emission in Nd^{3+}/Yb^{3+} co-doped $Ca_{12}Al_{14}O_{33}$ phosphor: Charge transfer state luminescence versus induced optical heating," *Chem. Phys. Lett.*, vol. 559, pp. 71–75, Feb. 2013.
[10] A. Speghini, F. Piccinelli, and M. Bettinelli, "Synthesis, characterization and luminescence spectroscopy of oxide nanopowders activated with trivalent lanthanide ions: The garnet family," *Opt. Mater.*, vol. 33, no. 3, pp. 247–257, Jan. 2011.
[11] J. E. Geusic, H. M. Marcos, and L. G. Van Uitert, "Laser oscillations in Nd-doped yttrium aluminum, yttrium gallium, and gadolinium garnets," *Appl. Phys. Lett.*, vol. 4, no. 10, pp. 182–184, 2010.
[12] M. P. Pechini, "*Method of preparing lead and alkaline earth titanates and niobates and coating method using the same to form a capacitor*, U.S. Patent, 3 330 697 A, 1967.

[13] G. Özen, J. Collins, M. Bettinelli, and B. Di Bartolo, "Luminescence of $Y_3Al_5O_{12}$ nano-particles doped with praseodymium ions," *Opt. Mater.*, vol. 35, no. 7, pp. 1360–1365, Mar. 2013.
[14] G. Zhao, T. Li, X. He, and J. Xu, "Preparation of gadolinium gallium garnet polycrystalline material by coprecipitation method," *Mater. Lett.*, vol. 56, no. 6, pp.1098–1102, Nov. 2002.
[15] P. Mazur, D. Hreniak, J. Niittykoski, W. Stręk, and J. Hölsä, "Formation of nanostructured Tb^{3+} doped yttrium aluminum garnets by the glycol route," *Mater. Sci.-Poland*, vol. 23, no. 1. pp. 261–268, 2005.
[16] M. Daldosso, D. Falcomer, A. Speghini, P. Ghigna, and M. Bettinelli, "Synthesis, EXAFS investigation and optical spectroscopy of nanocrystalline $Gd_3Ga_5O_{12}$ doped with Ln^{3+} ions $(Ln = Eu, Pr)$," *Opt. Mater.*, vol. 30, no. 7, pp. 1162–1167, Mar. 2008.
[17] M. Allibert, C. Chatillon, J. Mareschal, and F. Lissalde, "Étude du diagramme de phase dans le système $Gd_2O_3 - Ga_2O_3$," *J. Cryst. Growth*, vol. 23, no. 1, pp. 289–294, Oct. 1974.
[18] D. Hreniak, W. Stręk, P. Głuchowski, M. Bettinelli, and A. Speghini, "The influence of the specific surface grains on the luminescence properties of Nd^{3+}-doped $Y_3Al_5O_{12}$ nanopowders," *Appl. Phys. B*, vol. 91, no. 1, pp. 89–93, Apr. 2008.
[19] Y. N. Xu, W. Y. Ching, and B. K. Brickeen, "Electronic structure and bonding in garnet crystals $Gd_3Sc_2Ga_3O_{12}$, $Gd_3Sc_2Al_3O_{12}$, $Gd_3Ga_3O_{12}$ compared to $Y_3Al_3O_{12}$," *Phys. Rev. B*, vol. 61, no. 3, pp. 1817, Jan. 2000.
[20] J. P. Perdew, "Density functional theory and the band gap problem," *Int. J. Quantum Chem.*, vol. 28, no. S19, pp. 497–523, Mar. 1985.
[21] A. Matkovsky, D. Sugak, and Y. Kostikov, *Inorganic Material*, vol. 26, no. 4, 1990.
[22] W. Lotz, "Electron binding energies in free atoms," *J. Opt. Soc. Amer.*, vol. 60, no. 2, pp. 206–210, Feb. 1970.
[23] H. Örücü, G. Özen, B. Di Bartolo, and J. Collins, "Site-selective spectroscopy of garnet crystals doped with chromium ions," *J. Phys. Chem. A*, vol. 116, no. 15, pp. 8815–8826, Sep. 2012.
[24] G. Boulon, "Fifty years of advances in solid-state laser materials," *Opt. Mater.*, vol. 34, no. 3, pp. 499–512, Jan. 2012.
[25] B. Struve and G. Huber, "The effect of the crystal field strength on the optical spectra of Cr^{3+} in gallium garnet laser crystals," *Appl. Phys. B*, vol. 36, no. 4, pp. 195–201, Apr. 1985.
[26] A. Monteil, W. Nie, C. Madej, and G. Boulon, "Multisites Cr^{3+} in GGG and GSGG garnets," *Opt. Quant. Electron.*, vol. 22 pp. S247–S257, 1990.
[27] L. Kostyk, A. Luchechko, Y. Zakharko, O. Tsvetkova, and B. Kuklinski, "Cr-related centers in $Gd_3Ga_5O_{12}$ polycrystals," *J. Lumin.*, vol. 129, no. 3, pp. 312–316, 2009.
[28] S. Mahlik, B. Kukliński, M. Grinberg, L. Kostyk, and O. Tsvetkova, "Luminescence and luminescence kinetics of $Gd_3Ga_5O_{12}$, polycrystals doped with Cr^{3+} and Pr^{34}," *Acta Phys. Polonia A*, vol. 117, no. 1, pp. 117–121, 2010.
[29] N. L. Olenovich, G. A. Gromadskaya, and I. S. Anbinder, "Spectral determination of impurities in some aluminum compounds," *J. Appl. Spectr.*, vol. 23, no. 3, pp. 1161–1163, Sep. 1975.
[30] F. Vetrone, J.-C. Boyer, J. A. Capobianco, A. Speghini, and M. Bettinelli, "Luminescence spectroscopy and near-infrared to visible upconversion of nanocrystalline $Gd_3Ga_5O_{12}:Er^{3+}$," *J. Phys. Chem. B*, vol. 107, no. 39, pp. 10747–10752, 2003.
[31] J. A. Curcio and C. C. Petty, "The near infrared absorption spectrum of liquid water," *J. Opt. Soc. Amer.*, vol. 41, no. 5, pp. 302, May 1951.
[32] G. Bilir and B. Di Bartolo, "Production of bright, wideband white light from Y_2O_3 nano-powders induced by laser diode emission," *Opt. Mater.*, vol. 36, no. 8, pp. 1357–1360, Jun. 2014.
[33] G. Bilir and J. Liguori, "Laser diode induced white light emission of $\gamma - Al_2O_3$ nano-powders," *J. Lumin.*, vol. 153, pp. 350–355, Sep. 2014.